Am J Physiol Gastrointest Liver Physiol 316: G350–G365, 2019.
First published January 10, 2019; doi:10.1152/ajpgi.00080.2018.

RESEARCH ARTICLE | *Epithelial Biology and Secretion*

Dietary cholesterol and apolipoprotein A-I are trafficked in endosomes and lysosomes in the live zebrafish intestine

Jessica P. Otis,[1] Meng-Chieh Shen,[1] Blake A. Caldwell,[1] Oscar E. Reyes Gaido,[1,2] and Steven A. Farber[1,2]

[1]*Department of Embryology, Carnegie Institution for Science, Baltimore, Maryland; and* [2]*Department of Biology, Johns Hopkins University, Baltimore, Maryland*

Submitted 9 March 2018; accepted in final form 17 December 2018

Otis JP, Shen MC, Caldwell BA, Reyes Gaido OE, Farber SA. Dietary cholesterol and apolipoprotein A-I are trafficked in endosomes and lysosomes in the live zebrafish intestine. *Am J Physiol Gastrointest Liver Physiol* 316: G350–G365, 2019. First published January 10, 2019; doi:10.1152/ajpgi.00080.2018.—Difficulty in imaging the vertebrate intestine in vivo has hindered our ability to model nutrient and protein trafficking from both the lumenal and basolateral aspects of enterocytes. Our goal was to use live confocal imaging to increase understanding of intestinal trafficking of dietary cholesterol and apolipoprotein A-I (APOA-I), the main structural component of high-density lipoproteins. We developed a novel assay to visualize live dietary cholesterol trafficking in the zebrafish intestine by feeding TopFluor-cholesterol (TF-cholesterol), a fluorescent cholesterol analog, in a lipid-rich, chicken egg yolk feed. Quantitative microscopy of transgenic zebrafish expressing fluorescently tagged protein markers of early, recycling, and late endosomes/lysosomes provided the first evidence, to our knowledge, of cholesterol transport in the intestinal endosomal-lysosomal trafficking system. To study APOA-I dynamics, transgenic zebrafish expressing an APOA-I fluorescent fusion protein (APOA-I-mCherry) from tissue-specific promoters were created. These zebrafish demonstrated that APOA-I-mCherry derived from the intestine accumulated in the liver and vice versa. Additionally, intracellular APOA-I-mCherry localized to endosomes and lysosomes in the intestine and liver. Moreover, live imaging demonstrated that APOA-I-mCherry colocalized with dietary TF-cholesterol in enterocytes, and this colocalization increased with feeding time. This study provides a new set of tools for the study of cellular lipid biology and elucidates a key role for endosomal-lysosomal trafficking of intestinal cholesterol and APOA-I.

NEW & NOTEWORTHY A fluorescent cholesterol analog was fed to live, translucent larval zebrafish to visualize intracellular cholesterol and apolipoprotein A-I (APOA-I) trafficking. With this model intestinal endosomal-lysosomal cholesterol trafficking was observed for the first time. A new APOA-I fusion protein (APOA-I-mCherry) expressed from tissue-specific promoters was secreted into the circulation and revealed that liver-derived APOA-I-mCherry accumulates in the intestine and vice versa. Intestinal, intracellular APOA-I-mCherry was observed in endosomes and lysosomes and colocalized with dietary cholesterol.

apolipoprotein A-I; cholesterol; endosomes; lysosomes; zebrafish

INTRODUCTION

Cholesterol is a sterol lipid that provides structure and fluidity to cell membranes, serves as a precursor for bile acid and steroid hormone synthesis, and plays a key role in the etiology of cardiovascular disease (11, 20, 47, 54). It is known that dietary cholesteryl esters are hydrolyzed to free cholesterol in the intestinal lumen and then incorporated into micelles of dietary lipid and bile acids, which are absorbed by intestinal enterocytes (33). On the enterocyte brush border, cholesterol is internalized by the Niemann-Pick C1-like-1 transporter and delivered by an unknown mechanism to the endoplasmic reticulum (ER) where it is reesterified (2). After entering the cell, dietary cholesterol can be *1*) equilibrated with cellular cholesterol pools, *2*) resecreted into the intestinal lumen by the ATP-binding cassette transporters (ABCG5/G8) (54), *3*) reesterified and packaged by apolipoprotein B48 into chylomicrons and secreted into the lymph (23), or *4*) delivered to apolipoprotein A-I (APOA-I) by the ATP-binding cassette transporter ABCA1 on the basolateral enterocyte plasma membrane to form nascent high-density lipoprotein (HDL) particles (25).

Our understanding of intestinal cholesterol metabolism has been limited by a reliance on cultured cells, which cannot replicate the complex in vivo milieu that includes microbes, dietary nutrients, endocrine input, and bile. For example, the lumenal contents of the intestine affect cholesterol absorption: in the absence of lumenal dietary fatty acids, rats fail to internalize cholesterol (51, 57). The exact mechanism(s) by which lumenal fats promote cholesterol absorption remain(s) unknown. Additionally, the gut microbiome contributes to variations in blood lipid levels in humans independent of age, gender, and host genetics (14), and gnotobiotic zebrafish models have demonstrated that specific microbes promote intestinal lipid absorption (44).

In addition to questions regarding how lumenal contents affect cholesterol absorption, the cell biology of enterocyte intracellular processing remains mysterious (e.g., how does cholesterol imported into the cell by Niemann-Pick C1-like-1 reach the ER?) (21). In several other cell types, including hepatocytes, cholesterol derived from exogenous sources is imported through the endosomal-lysosomal trafficking system (31, 49). Lysosomes are classically known for their degradative capacity, conferred by acidic pH and hydrolytic enzymes, and hence their contributions to lipid catabolism (45). However, it has historically been difficult to determine if cholesterol is transported in endosomes and lysosomes in enterocytes be-

Address for reprint requests and other correspondence: S. A. Farber, Dept. of Embryology, 3520 San Martin Dr., Baltimore, MD 21218 (e-mail: farber@carnegiescience.edu).

cause of the lack of animal models and techniques to observe cholesterol transport in the live intestine.

The shortage of models to observe intracellular transport in the live intestine has impeded not only the study of cholesterol trafficking but also of apolipoprotein and lipoprotein biology in enterocytes. Moreover, the majority of HDL research has focused on the protective effects of HDL in the circulation, leaving the intracellular events that greatly influence circulating APOA-I and HDL levels and functionality undefined. Although a small body of literature has established that HDL particles can be internalized and APOA-I/HDL can be found in endosomes and lysosomes (22, 24, 38, 39, 53, 55), these localizations have not been confirmed in vivo. Interestingly, despite its localization to lysosomes, internalized HDL experiences only limited degradation in multiple types of cultured cells (38, 48), supporting speculation that HDL is internalized for a primary purpose other than degradation. Moreover, how APOA-I and HDL may be modified during intracellular trafficking remains unclear (1, 8, 13, 35). The hypothesis that endosomes may be a depot for the extraction of HDL cholesterol is supported by the observation that HDL particles contained less cholesterol following resecretion from HepG2 cells (41).

In this study we employed the strengths of the optically clear, genetically tractable larval zebrafish to address several long-standing questions regarding dietary cholesterol and apolipoprotein internalization, transport, and localization in the intestine and liver. Morphological similarities between the zebrafish and human gastrointestinal system, as well as the as the high degree of genetic conservation in apolipoproteins, make the zebrafish an ideal model for the study of lipid biology (5, 37). Here we report an array of new tools to study the cellular and molecular biology of lipids and their associated proteins in cells within a living organ. Using this system, we characterize a poorly understood intracellular pool of intracellular APOA-I, showing that it colocalizes with dietary cholesterol in endosomes and lysosomes within the live intestine.

MATERIALS AND METHODS

Zebrafish husbandry and maintenance. All zebrafish research was approved by the Carnegie Institution Animal Care and Use Committee. Adult zebrafish (AB background) were maintained at 28.5°C on a 14-h:10-h light-dark cycle and fed either two times per day with shell-free Artemia (decapsulated, nonhatching) and Hikari Micropellets or one time per day with Gemma Micro 300 pellets. Embryos were obtained by natural spawning, staged as described by Kimmel et al. (26), and raised in embryo medium (EM) at 28.5°C on a 14-h:10-h light-dark cycle until 6 days postfertilization (dpf). Zebrafish were not provided exogenous food before 6-dpf. Larval zebrafish cannot be sexed at the 6-dpf stage as they do not have sex chromosomes and do not develop into males or females until the juvenile stage. All experiments were performed on 6-dpf larvae.

Generation of transgenic zebrafish. Transgenic zebrafish were generated as described previously with the Tol2-Gateway molecular cloning system (27). Zebrafish have two apoA-I paralogs: *apoA-Ia* is expressed in the intestine whereas *apoA-Ib* is expressed in the intestine and liver at 6-dpf (37). Zebrafish *apoA-Ia* (*zapoA-Ia*) was cloned from cDNA prepared from 6-dpf larvae with the following primers: forward (F): GGG GAC AAG TTT GTA CAA AAA AGC AGG CTT TAC CAT GAA AGC TGC GGT GCT G and reverse (R): GGG GAC CAC TTT GTA CAA GAA AGC TGG GTT CTG GGT GTT GAG CTT CTT. Human *APOA-I* (h*APOA-I*) was cloned from an Open Biosystems h*APOA-I* clone (ID LIFESEQ2516350) with the following primers: F: GGG GAC AAG TTT GTA CAA AAA AGC AGG CTC CAC CCA GCA CCT CTC AGG GCT TAA TC and R: GGG GAC CAC TTT GTA CAA GAA AGC TGG GTT TGC CTG GAT GGC CTT GG. Both constructs introduced a Kozak sequence (ACC) and were cloned into the pDONR221 middle-entry vector with BP clonase. A geneblock of the zebrafish *lamp1* gene containing a Kozak sequence (GCAAAC), 3′ Gateway ATTL1 sequence, and 5′ ATTL2 sequence was purchased (Integrated DNA Technologies, Coralville, IA). The intestine-specific intestinal fatty acid binding protein (*ifabp*) promoter was provided by Michel Bagnat; the liver-specific liver fatty acid binding protein 10 (*lfabp10*) promoter (−2.8 kb), p3E *rab5c*, p3E *rab11a*, and p3E *rab7* were provided by Brian Link (10), and the β-actin2 (*bactin2*) promoter, heat shock cognate 70-kDa protein, like (*hsp70l*) promoter, p3E-eGFPpA, p3E-mCherrypA, pME-eGFP no stop, and pME-mCherry no stop plasmids were originally provided by Chi-bin Chien. Gateway recombination was used to combine these entry vectors into the pDestTol2Pa2 plasmid creating the full transgene constructs listed in Table 1.

Stable transgenic zebrafish lines were generated by injecting 50 pg of the constructs and 40 pg tol2 transposase mRNA into 1–2-cell embryos, raising the zebrafish to adulthood, and screening for progeny stably expressing the fluorescent construct. Transgenic larvae expressing a heat shock-inducible construct were heat-shocked at 37°C in 15 ml EM for 45 min at 5-dpf and screened for whole body fluorescence at 6-dpf. The other transgenic zebrafish were screened for fluorescence at 5- or 6-dpf. All experiments in transgenic zebrafish were performed on three independent stable lines, with the exception of *tg(hsp70l:lamp1-eGFP)* transgenics, which were of the F0 generation.

Preparation of chicken egg feeds. Chicken egg liposome feeds were prepared as described previously (4, 36). Briefly, 5% chicken egg yolk or white feeds were made by adding egg yolk or egg white to EM and vortexing vigorously for 30 s. The emulsion was sonicated (Ultrasonic Processor 3000, Misonix, Inc., Farmingdale, NY) with a one-quarter-inch tapered microtip for 40 s total (settings: 1 s on, 1 s off, total of 5 s; output intensity of 3 W).

TopFluor-cholesterol feed. Dipyrromethene difluoride-cholesterol, or TopFluor-cholesterol (TF-cholesterol) (810255P, Avanti Polar Lipids, Inc., Alabaster, AL), is a widely used fluorescent cholesterol analog (19). TF-cholesterol was incorporated into the chicken egg yolk and white liposomes. TF-cholesterol was prepared as a 1.5 μg/μl stock in chloroform; 8 μl was dried under nitrogen, resuspended in 15 μl room-temperature ethanol, and mixed with 85 μl of 1% fatty acid-free BSA (at 30°C). The TF-cholesterol solution was combined with 5 ml of the 5% egg yolk feed (at 30°C) and vortexed for 30 s to result in a final concentration of 2.4 μg/ml TF-cholesterol. Larvae were fed for 3, 4, or 6 h.

BODIPY TR ceramide feeds. For boron dipyrromethene fluorophore (BODIPY) TR ceramide (D-7540, ThermoFisher Scientific) labeling experiments, an aliquot from a chloroform stock was dried under nitrogen, reconstituted in ethanol and 1% FA-free BSA as

Table 1. *Transgenic zebrafish generated by Gateway cloning*

Transgenic Zebrafish
tg(lfabp10:hAPOA-I-mCherry)
t*g(lfabp10:zApoA-Ia-mCherry*)
tg(ifabp:hAPOA-I-mCherry)
tg(ifabp:zApoA-Ia-mCherry)
tg(β-actin2:eGFP-rab5c)
tg(β-actin2:eGFP-rab7)
tg(β-actin2:eGFP-rab11a)
tg(β-actin2:mCherry-rab5c)
tg(β-actin2:mCherry-rab7)
tg(β-actin2:mCherry-rab11a)
tg(hsp70l:lamp1-eGFP)

above, and emulsified in 0.5% chicken egg yolk liposomes for a final concentration of 5 μg/ml BODIPY TR ceramide. Larvae were fed for 4 h.

Larval zebrafish feeding protocol. Larvae that had been prewarmed to 30°C for ~15 min were introduced to the chicken egg yolk emulsions and allowed to feed in a 30°C shaking incubator (Incu-Shaker Mini, Benchmark, Edison, NJ). Following feeding, larvae were washed three times in EM, anesthetized with tricaine (Argent Chemical, Redmond, WA), and screened for the presence of food in the intestine.

LysoTracker staining. LysoTracker staining was performed as previously reported (18). Larvae were soaked in 10 μM LysoTracker Deep Red (L12492,ThermoFisher Scientific) in EM for 1 h with gentle shaking and washed with EM three times.

Live confocal microscopy. Larvae anesthetized with tricaine were mounted in 3% methyl cellulose by the coverslip lean-to method and imaged with a 6×63/numerical aperture 1.4 oil immersion objective on a Leica DM6000 upright or Leica DMI6000 inverted microscope with a Leica TCS-SP5 confocal scanner with photomultiplier detectors (36). Zebrafish were imaged with an argon laser using a 4-line average, and the fluorescence intensity of the confocal images was recorded with 12-bit dynamic range. Only 1–2 images were captured per larvae to minimize bleaching.

Quantitative image analysis. The areas of TF-cholesterol, enhanced green fluorescent protein (eGFP), and mCherry fluorescence were quantified with Metamorph software (Molecular Devices, Sunnyvale, CA). One image was analyzed per fish. First, five cells (enterocytes or hepatocytes) were manually outlined to define cell borders and saved as region files. Second, to segment regions of interest containing fluorescence above background (noise and autofluorescence), 5×5 low-pass and morphological top hat filters were applied. Third, for both the TF-Cholesterol/eGFP and mCherry channels, the total areas positive for fluorescence in the regions of interest and the total area of overlap were reported.

Western blot analysis. Total protein lysates from larvae (6-dpf) were prepared by homogenizing in protein extraction buffer (T-PER Tissue Protein Extraction Reagent, Thermo Scientific, cat. no. 78510) supplemented with protease inhibitor (cOmplete Mini, EDTA Free Protease inhibitor, Roche, Indianapolis, IA, cat. no. 04693159001) followed by determination of protein concentration (BCA assay). SDS-PAGE gels (Mini-Protean system, Bio-Rad, Hercules, CA) were loaded with 30 μg of total protein. Two loading buffers were used depending on the antibody and assay performed: denaturing buffer A: 2% SDS, 5 mM Tris·HCl (pH 6.8), 5% betamercaptoethanol, 5% glycerol, and 0.05% bromophenol blue; higher detergent denaturing buffer B: 3% SDS, 62.5 mM Tris·HCl (pH 6.8), 5% betamercaptoethanol, 5% glycerol, and 0.05% bromophenol blue. Samples diluted in buffer A were denatured by boiling for 5 min, whereas samples treated with loading buffer B were heated at 37°C for 15 min. For samples diluted in buffer B and probed with APOA-I antibody, further denaturation after membrane transfer was required (membranes were placed in a beaker filled with minimal water and autoclaved for 15 min) (50). After transferring, blots were blocked with 5% nonfat milk in Tris-buffered saline-Tween 20 [50 mM Tris·HCl (pH 7.5),150 mM NaCl, 0.05% Tween 20] for 1 h at room temperature. Antibodies were diluted in 2.5% nonfat milk with Tris-buffered saline-Tween 20 as indicating dilution. Goat anti-ApoA1 (1:500; Rockland, cat. no. 600-101-109), rabbit anti-mCherry (1:1,000; Abcam, cat. no. ab-167453), goat anti-rabbit IgG(H^+L)-horseradish peroxidase (1:3,000, Bio-Rad, cat. no. 170-6515), and donkey anti-goat-horseradish peroxidase (1: 3,000, Santa Cruz Biotechnology, cat. no. sc-2056) protein expression was detected by chemiluminescence (SuperSignal West Pico Chemiluminescent Substrate, cat. no.34580, Pierce, Rockford, IL) and imaged with LI-COR Odyssey Fc imaging system (10-min exposure).

Imaging ApoA-I-mCherry fluorescence using native protein gel electrophoresis. Zebrafish larvae (6-dpf) were homogenized in native gel lysis buffer [50 mM Tris·HCl (pH 7.5), 25 mM NaCl, 1 mM EDTA, 0.1% TritonX-100) with protease inhibitor (cOmplete Mini, EDTA Free Protease inhibitor, Roche, cat. no. 04693159001] and mixed with 5× loading dye (40% sucrose, 0.02% bromophenol blue). Five and a half larvae were loaded per well and were run on a 6% native gel (6% polyacrylamide, 89 mM Tris base, 89 mM boric acid, 20 mM EDTA). Gel fluorescence was determined using LI-COR Odyssey Fc imaging system 600 nm channel (10-min exposure).

Whole mount immunofluorescence. Endogenous ApoA-Ia and ApoA-Ib protein expression was localized with whole mount immunofluorescence. Zebrafish (6-dpf) were fixed overnight in 4% paraformaldehyde, probed with APOA-I antibody (cat. no. 600-101-109, Rockland Antibodies and Assays; 1:50 dilution), secondary donkey-anti-goat Alexa Fluor 488 conjugate (cat. no. A-11055, Life Technologies, Carlsbad, CA; 1:250 dilution), and imaged on an upright Leica SP5 confocal microscope as described above.

In situ hybridization. mCherry mRNA expression was assessed by whole mount in situ hybridization as previously described (52) for each of the following transgenic zebrafish: *Tg(lfabp10:hAPOA-I-mCherry*), *Tg(lfabp10:zapoA-Ia-mCherry*), *Tg(ifabp:hAPOA-I-mCherry*), and *Tg (ifabp:zapoA-Ia-mCherry*). Larvae were fixed in 4% paraformaldehyde overnight. A probe specific to mCherry was amplified from cDNA from the p3E-mCherrypA plasmid with previously published primers (42), TOPO cloned into pCRII (Invitrogen, Grand Island, NY), and used to generate sense and antisense digoxigenin-labeled riboprobes (digoxigenin: Roche) that were hybridized to 6-dpf zebrafish ($n = 10–12$).

Statistical analysis. The mean fluorescence intensities of TF-cholesterol in enterocytes following egg yolk or egg white feeds were compared by Student's *t*-test. The TF-cholesterol and mCherry-Rab fusion protein fluorescence colocalization and their overlap were analyzed by one-way ANOVA of samples performed either at the same feeding time point or with the same mCherry-Rab fusion. The eGFP-Rab fusion and hAPOA-I-mCherry fluorescence colocalization and overlap were analyzed by one-way ANOVA of samples within the same hAPOA-I-mCherry transgenic line, with one exception: the percent of eGFP-Rab fusion fluorescence colocalized to hAPOA-I-mCherry fluorescence in enterocytes was compared by two-way ANOVA of all groups. TF-cholesterol and hAPOA-I-mCherry fluorescence colocalization and overlap were analyzed by one-way ANOVA of samples within the same APOA-I-mCherry transgenic line. Barlett's or Brown-Forsythe tests confirmed homogeneity of variance for data evaluated by ANOVA. Statistics were carried out with Prism software (GraphPad, La Jolla, CA).

RESULTS

Assay to image dietary cholesterol absorption in live zebrafish verifies that lumenal lipids are necessary for dietary cholesterol absorption. We developed an assay to visualize dietary cholesterol absorption and accumulation in enterocytes of live zebrafish larvae. When zebrafish were fed the cholesterol analog TF-cholesterol in a lipid-rich, chicken egg yolk emulsion and subject to confocal microscopy 3 h following the onset of feeding distinct subcellular punctae within intestinal enterocytes were observed (Fig. 1*A*). By contrast, little fluorescence was absorbed when TF-cholesterol was fed in a lipid-poor, chicken egg white feed (Fig. 1*B*). Quantification of these images demonstrated that the mean fluorescence intensity of TF-cholesterol within enterocytes was ~sixfold higher when it was provided with a lipid-rich, compared with a lipid-poor, feed (Student's *t*-test, $*P < 0.05$; Fig. 1*C*). We next set out to characterize the specific subcellular compartments labeled by TF-cholesterol.

Dietary cholesterol observed in the endosomal-lysosomal trafficking system in enterocytes. Various types of endosomes can be identified by the presence of specific small GTPases

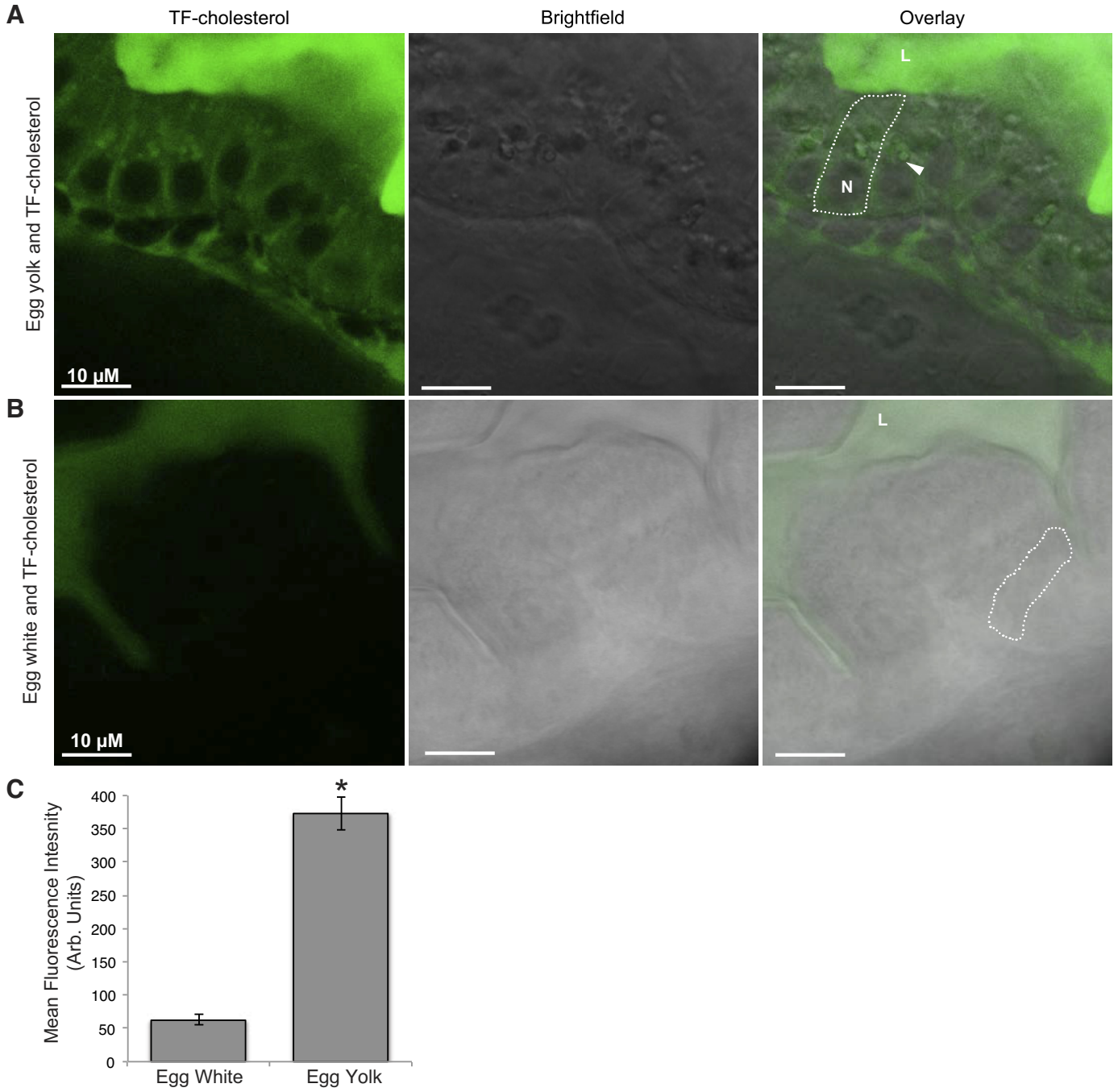

Fig. 1. Visualization of TF-cholesterol absorption in live, larval zebrafish indicates fatty acids are necessary for dietary cholesterol absorption. TF-cholesterol provided in a lipid-rich meal (5% chicken egg yolk) is absorbed by enterocytes and accumulates in distinct subcellular punctae (*A*). Representative images show that dietary TF-cholesterol absorption is not observed when it is fed with a lipid-poor meal (5% chicken egg white) (*B*). Approximately sixfold more TF-cholesterol fluorescence is observed in enterocytes when it is provided with egg yolk relative to egg white (*C*) (means ± SE, student's *t*-test, $*P < 0.05$). $n = 3$, with 6–9 fish per *n*. Arrows indicate colocalization; L, intestinal lumen; N, nucleus; TF-cholesterol, TopFluor-cholesterol.

known as Rab proteins (15). Early, or sorting, endosomes, receive the products of endocytosis and can be recognized by the presence of RAB5 (17). Early endosomal contents can be sorted to recycling endosomes, marked by RAB11, which target their contents for exocytosis (34). Alternatively, early endosomal contents can be sorted to acidic late endosomes, marked by RAB7. These late endosome may then mature into, or fuse with, highly acidic lysosomes, which are also marked by RAB7 (32). To determine if dietary cholesterol accumulates in the endosomes and lysosomes of enterocytes following lumenal absorption, TF-cholesterol was fed in 5% egg yolk to three different transgenic zebrafish lines expressing fluorescently tagged markers of early (mCherry-Rab5c), recycling (mCherry-Rab11a), and late endosomes/lysosomes (mCherry-Rab7). Live imaging of zebrafish expressing mCherry-Rab5c revealed colocalization of dietary TF-cholesterol to early en-

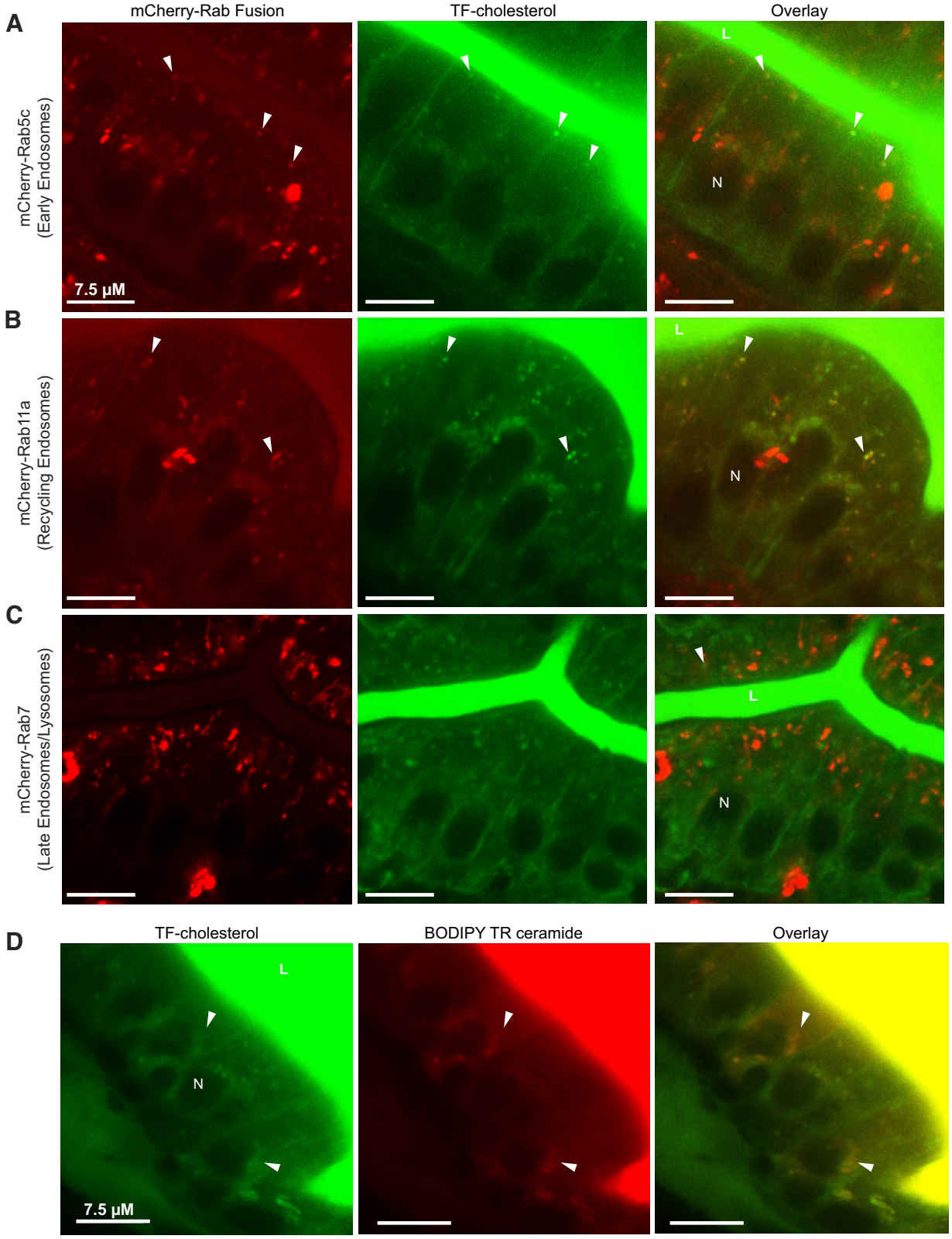

Fig. 2. Dietary TF-cholesterol localizes to the endosomal-lysosomal trafficking network in enterocytes. Representative images show that 3 h following the onset of feeding, dietary TF-cholesterol colocalizes to mCherry-Rab5c (early endosomes) (*A*), mCherry-Rab11a (recycling endosomes) (*B*), and mCherry-Rab7 (late endosomes) (*C*). $n = 3$, with 3–9 fish per n; all fish 6-dpf. TF-cholesterol colocalizes with BODIPY TR ceramide, which marks the trans-Golgi network, in enterocytes after 4 h of feeding (*D*). $n = 3$, with 3–6 fish per n. Arrows indicate colocalization; dpf, days postfertilization; L, intestinal lumen; N, nucleus; TF-cholesterol, TopFluor-cholesterol.

dosomes following 3 h of lipid feeding (Fig. 2*A*). Similarly, larvae expressing mCherry-Rab11a displayed colocalization with dietary TF-cholesterol in recycling endosomes (Fig. 2*B*), and larvae expressing mCherry-Rab7 indicated colocalization in late endosomes and lysosomes (Fig. 2*C*). Imaging at later time points after feeding (4 and 6 h) revealed continued colocalization between dietary TF-cholesterol and all of these endomembrane domains (data not shown). Dual feeds with the Golgi marker TopFluor-ceramide and TF-cholesterol established colocalization of dietary cholesterol to the Golgi 4 h after the onset of feeding (Fig. 2*D*).

Images of the live larvae at 3, 4, and 6 h of feeding were quantified to determine the percent of TF-cholesterol fluorescence that colocalized with mCherry-Rab fusion fluorescence, the percent of mCherry-Rab fusion fluorescence that colocalized with TF-cholesterol fluorescence, and the area of TF-cholesterol and mCherry-Rab fusion overlap. After 3 h of feeding, a greater percent of TF-cholesterol fluorescence colocalized to early endosomes (44.7%) than late endosomes/lysosome (22.1%) or recycling endosomes (20.3%) (1-way ANOVA, $F = 7.274$, $P < 0.05$; Fig. 3*A*). Additionally, a significantly greater percent of TF-cholesterol fluorescence colocalized

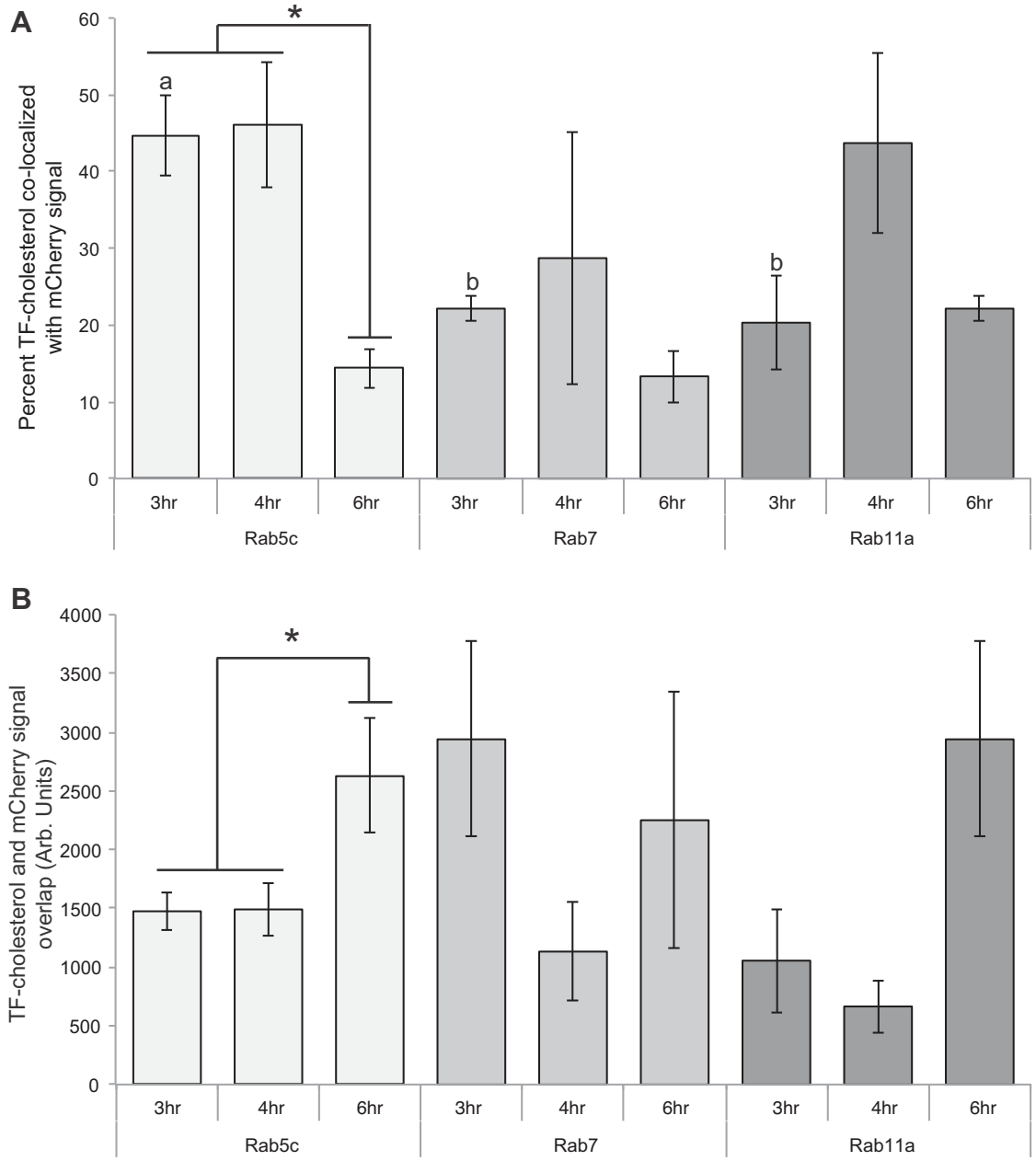

Fig. 3. Quantification of dietary TF-cholesterol colocalizes to endosomes and lysosomes in enterocytes. *A*: a greater percent of TF-cholesterol colocalizes to early endosomes (mCherry-Rab5c) at 3 and 4 h following the onset of feeding than at 6 h (means ± SE, 1-way ANOVA of mCherry-Rab5c groups, $*P < 0.01$). At 3 h into feeding, a greater percent of TF-cholesterol colocalizes to early endosomes (mCherry-Rab5c) than late (mCherry-Rab7) or recycling (mCherry-Rab11a) endosomes (means ± SE, 1-way ANOVA of 3-h groups, groups with different letters are significantly different $*P < 0.05$, $n = 3$–5, with 3–9 fish per n). *B*: area of TF-cholesterol and mCherry-Rab5c fluorescence overlap increases over feeding time (means ± SE, 1-way ANOVA of mCherry-Rab5c groups, $*P < 0.01$, 1-way ANOVA of mCherry-Rab11a groups $P = 0.0511$ $n = 3$–5, with 3–9 fish per n). TF-cholesterol, TopFluor-cholesterol.

to early endosomes at 3 and 4 h (44.7 and 46.0%), than 6 h (14.4%) (1-way ANOVA, $F = 7.772$, $P < 0.01$; Fig. 3*A*), but the area of TF-cholesterol and early endosome overlap was greater at 6 h of feeding (2,630 arbitrary units), than 3 or 4 h (1,477.7 and 2,630.8 arbitrary units) (1-way ANOVA, $F = 4.721$, $P < 0.01$; Fig. 3*B*). Finally, when all groups were compared, there is a significant effect of time on the percent of TF-cholesterol fluorescence colocalized to mCherry-Rab fluorescence (2-way ANOVA, $F_{(2,24)} = 6.379$, $P < 0.01$; Fig. 3*A*) and the total area of TF-cholesterol and mCherry-Rab overlap (2-way ANOVA, $F_{(2,24)} = 5.778$, $P < 0.01$).

Visualization of APOA-I in live zebrafish: APOA-I-mCherry derived from the liver accumulates in the intestine and APOA-I-mCherry derived from the intestine accumulates in the liver. As part of an effort to understand the intracellular role of ApoA1, we generated transgenic zebrafish expressing APOA-I fused to the mCherry fluorescent protein under the control of tissue-specific promoters. Specifically, we set out to visualize APOA-I in live, larval zebrafish by creating a novel fluorescent fusion protein: hAPOA-I-mCherry that was expressed using liver- or intestinal-specific promoters (*lfabp10* and *ifabp*, respectively; Fig. 4). As described in the methods, we also created a zebrafish fusion protein (zAPOA-I-mCherry) that exhibited very similar subcellular localizations (Fig. 5). Live confocal microscopy revealed that hAPOA-I-mCherry was secreted from their tissue of synthesis and localized to subcellular compartments of several tissues, including the intestine and liver (Fig. 4). Imaging of *tg(lfabp10:hAPOA-I-mCherry)* larvae (6-dpf) revealed that APOA-I-mCherry of hepatic origin accumulates in intestinal enterocytes (Fig. 4, *A*–C). Similarly, imaging of *tg(ifabp:hAPOA-I-mCherry)* larvae revealed that APOA-I of intestinal origin are taken up and accumulate in the liver (Fig. 4, *E*–F). Whole mount in situ hybridization for mCherry mRNA in stable transgenic fish verified the tissue specificity of these promoters (all 10–12 larvae probed showed the same, tissue-specific expression) (Fig. 4, *D* and *G*).

To verify that the subcellular fluorescence is produced by the APOA-I-mCherry full-length fusion protein and not a degradation product, we performed a number of immunoblots and native protein analyses of protein lysates from transgenic larvae. Using a standard immunoblotting protocol with hAPOA-I antibody on lysates of *Tg(lfabp10:hAPOA-I-mCherry)* and *Tg(ifabp:hAPOA-I-mCherry)* (loading buffer A, boiled 5 min), a predominate, single APOA-I-mCherry band with a molecular mass of 50 kDa was observed; the predicted fusion protein weight is 56 kDa (both mCherry and ApoA-each typically run at ~28 kDa on SDS-PAGE gels) (Fig. 4*H*). No immunoreactive band was detected in wild-type animals (the hAPOA-I antibody does not react with endogenous zApoA-I). Paradoxically, when we probed with mCherry antisera, no band was shown at 50 kDa; instead two bands of an apparent molecular weight of around 25 kDa were detected. To test the hypothesis that the denatured APOA-I-mCherry fusion protein masked the mCherry antibody epitope, two additional experiments were performed.

Using a protocol optimized for an ApoA-I-interacting protein (ABCA1) that also binds lipids, we used a loading buffer containing more SDS coupled with gentle heating (loading buffer B; heated at 37°C for 15 min). Under these conditions, mCherry antisera revealed two distinct bands consistent with both full-length APOA-I-mCherry (50 kDa) and free mCherry [25 kDa, the identical size detected from *Tg(ef1a: mCherry-CVLL)*] (Fig. 4*I*). However, when using loading buffer B, no APOA-I immunoreactivity was detected. This result indicates that the APOA-I epitope requires the more stringent denaturing conditions used in standard protein immunoblot protocols. Consistent with this result, mCherry antisera can detect the APOA-I-mCherry full-length fusion protein in lysates prepared in buffer B when the blot is autoclaved immediately after transfer (data not shown). Analysis of the mCherry blots of *Tg(lfabp10:hAPOA-I-mCherry)* larvae reveals about a quarter of the mCherry is expressed as fusion protein, and the rest is significantly truncated. In *Tg(ifabp:hAPOA-I-mCherry)*, a majority of mCherry is expressed as a full-length fusion protein.

To test whether the bands detected by the mCherry antisera were fluorescent, we subjected lysates to native gel electrophoresis and then directly measured fluorescence (Fig. 4*J*). We observed a single fluorescent band from *Tg(ifabp:hAPOA-I-mCherry)* larval extracts consistent with the APOA-I-mCherry fusion protein and three distinct bands from *Tg(lfabp10:hAPOA-I-mCherry)* (60% APOA-I-mCherry fusion protein and 40% in the lower-size bands). Although we do observe evidence of fluorescent degradation products from both lines, it is a greater proportion when expressed from the liver-specific promoter.

To determine if subcellular ApoA-I accumulations in digestive organs analogous to the fluorescent puncta observed using APOA-I-mCherry zebrafish lines could be detected in non-transgenic zebrafish, whole mount immunohistochemistry was performed on fixed larval zebrafish. Although the hAPOA-I antisera fails to detect endogenous zebrafish protein on immunoblots, similar immunoreactive puncta were observed using the hAPOA-I antisera (Fig. 4*K*). No immunoreactive signal was observed in negative control samples lacking APOA-I antisera (data not shown).

Fig. 4. Transgenic zebrafish allows for visualization of human APOA-I in vivo. Live *tg(lfabp10:hAPOA-I-mCherry)* (*A*–*C*) and *tg(ifabp:hAPOA-I-mCherry)* (*E*–*F*) larvae show hAPOA-I-mCherry accumulation in the liver and intestine. hAPOA-I-mCherry derived from the liver (outlined by dotted line) accumulates in the intestine outlined by wavy line) and hAPOA-I-mCherry derived from the intestine accumulates in the liver (*B* and *C*). Tissue specificity of promoters used in APOA-I-mCherry transgenic fish revealed using whole mount in situ hybridization with antisense riboprobes to mCherry mRNA (*D* and *G*). No expression was detected with the sense probes ($n = 10$–12 fish); all larvae 6-dpf. ApoA-I-mCherry fusion protein is made in transgenic zebrafish and partially degraded (*H*). ApoA-I-mCherry fusion protein (arrow head) is made in transgenic zebrafish as expected size (50 kDa) (representative image from three experiments). mCherry antisera detected two different bands from Tg(lfabp:hApoA-I-mcherry) and Tg(ifabp:hApoA-I-mcherry) (*I*). The higher molecular weight bands (arrow head) represent ApoA-I-mCherry full-length protein. The lower molecular weight bands (arrow) is possibly a degradation product of similar size as mCherry protein made from Tg(ef1a:mcherry-CVLL) (representative image from two experiments). mCherry flourscence on native gel (representative image from four experiments) (*J*). Immunofluorescence for endogenous zApoA-Ia and zApoA-Ib in wild-type fish show punctae within the intestine similar to hAPOA-I-mCherry accumulation (representative image from three experiments) (*K*). APOA-I, apolipoprotein A-I; dpf, days postfertilization; E, Tg(ef1a:mcherry-CVLL); hAPOA-I, human APOA-I; I, Tg(ifabp:hApoA-I-mcherry); L, Tg(lfabp:hApoA-I-mcherry); W, wild-type; zAPOA-1, zebrafish APOA-1.

In vivo evidence that APOA-I is transported in endosomes and localizes to lysosomes. To determine whether internalized APOA-I localizes with endosomes and lysosomes *tg(lfabp10:hAPOA-I-mCherry)* and *tg(ifabp:hAPOA-I-mCherry)* zebrafish were crossed to the transgenic zebrafish described previously (10) that express endosomal/lysosomal markers. Live imaging provided the verification that hAPOA-I-mCherry derived from both the liver and intestine localized to early, recycling, and

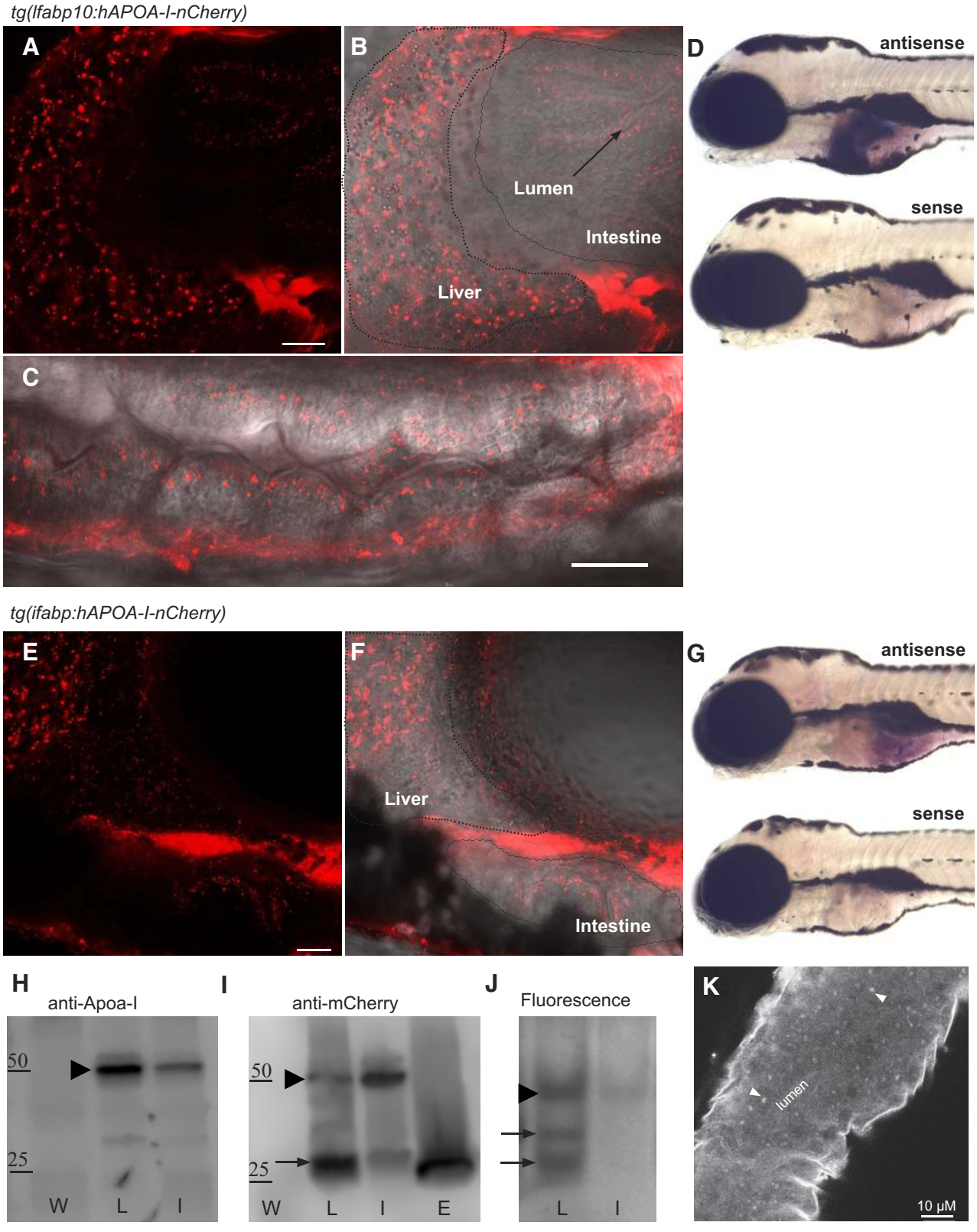

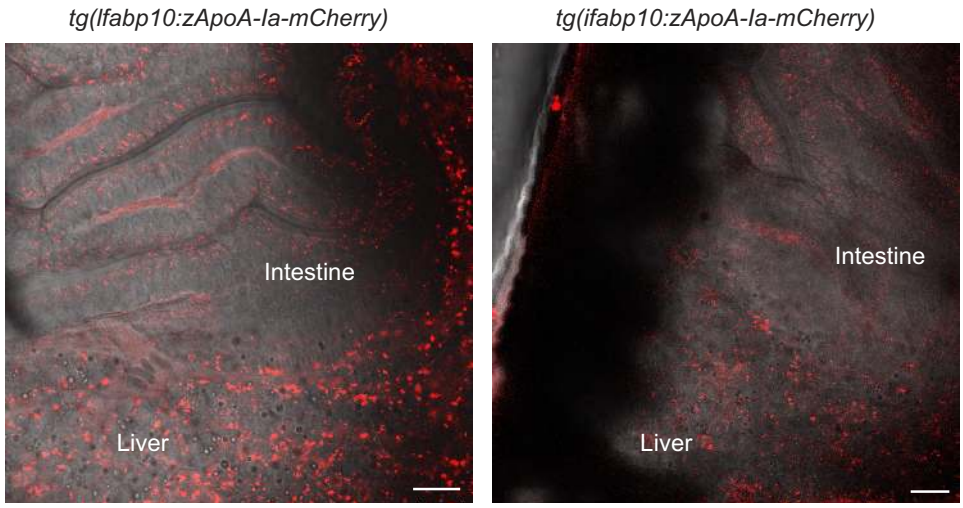

Fig. 5. Transgenic zebrafish allows for visualization of zebrafish APOA-Ia in vivo. Live *tg(lfabp10:zApoA-Ia-mCherry)* (*left*) and *tg(ifabp:zApoA-Ia-mCherry)* larvae show APOA-I-mCherry accumulation in the liver and intestine (*right*). Scale bar = 20 μm, all larvae 6-dpf. APOA-I, apolipoprotein A-I; dpf, days postfertilization.

late endosomes, as well as lysosomes, in enterocytes (Fig. 6 and 7) and hepatocytes (data not shown) in vivo. Further evidence for hAPOA-I-mCherry localization to lysosomes was provided by colocalization of hAPOA-I-mCherry derived from both tissues to LysoTracker (Fig. 6*D*), which stains acidic compartments, including late endosomes and lysosomes, and Lamp1-eGFP (Fig. 7*D*), which specifically marks lysosomes.

In enterocytes of both *tg(ifabp:hAPOA-I-mCherry)* and *tg(lfabp10:hAPOA-I-mCherry)* fish, twice as much hAPOA-I-mCherry signal localizes to late endosomes/lysosomes than early or recycling endosomes [*tg(ifabp:hAPOA-I-mCherry)*: 1-way ANOVA, $F = 19.71$, $P < 0.005$; *tg(lfabp10:hAPOA-I-mCherry)*: 1-way ANOVA, $F = 12.59$, $P < 0.005$] (Fig. 8*A*). In hepatocytes of *tg(lfabp10:hAPOA-I-mCherry)* larvae, the percent of hAPOA-I-mCherry signal in late endosomes/lysosomes was similarly greater than the percent in early endosomes or recycling endosomes (1-way ANOVA, $F = 11.33$, $P < 0.005$; Fig. 8*B*).

APOA-I-mCherry colocalizes with dietary TF-cholesterol in enterocytes. Because the previous results indicated that both dietary TF-cholesterol and hAPOA-I-mCherry are independently found in the endosomal-lysosomal trafficking system, we next assayed whether liver-derived hAPOA-I-mCherry colocalized with dietary cholesterol in these compartments of enterocytes. Indeed, hAPOA-I-mCherry and TF-cholesterol colocalization was observed in enterocytes of *tg(lfabp10:hAPOA-I-mCherry)* larvae upon feeding a lipid-rich meal (5% egg yolk) for 3, 4, and 6 h (Fig. 9). Quantification of these images found that the percent of TF-cholesterol in enterocytes that colocalized with hAPOA-I-mCherry in *tg(lfabp10:hAPOA-I-mCherry)* larvae increased from 12.1% at 3 h of feeding to 21.6% at 6 h of feeding (1-way ANOVA, $F = 4.587$, $P < 0.05$; Fig. 9*D*). Likewise, the area of TF-cholesterol and APOA-I-mCherry overlap increased with feeding time, nearly doubling at 6 h (data not shown). These trafficking data are consistent with a role for intracellular ApoA-I in dietary cholesterol trafficking.

DISCUSSION

We developed an assay to image dietary cholesterol in the live zebrafish intestine. In conjunction with zebrafish expressing Rab fluorescent fusion proteins, this assay reveals that dietary cholesterol colocalizes with intestinal endosomes and lysosomes. Furthermore, a novel APOA-I-mCherry fluorescent fusion protein demonstrates that APOA-I is trafficked in endosomes and also localizes to lysosomes in the intestine and liver. Our use of tissue-specific promoters to express APOA-I-mCherry elucidated some of the first descriptions of cellular uptake and accumulation of APOA-I derived from specific tissues. In this way, it was appreciated that the intestine internalizes APOA-I derived from the liver and vice versa. Moreover, we demonstrated that APOA-I-mCherry colocalizes with dietary cholesterol within enterocytes.

In 2011, our laboratory reported an assay that incorporated fluorescent fatty acid analogs into a lipid-rich chicken egg yolk feed to visualize dietary fatty acid absorption in the intestine and accumulation throughout the body (4). Here, we extended the power of that assay to a new class of lipids by incorporating a fluorescent cholesterol analog into the chicken egg yolk feed. This TF-cholesterol feeding assay was in part validated by its ability to reproduce the long appreciated but still enigmatic requirement of lumenal triglycerides and fatty acids for cholesterol absorption (51, 57).

Although our static observations of TF-cholesterol at three time points after feeding are consistent with it being trafficked through the endosomal/lysosomal system, we cannot rule out that TF-cholesterol gets incorporated directly into ER lipid pools that then distributes to all membrane compartments. Time-lapse and pulse-chase studies may be able to resolve these two possibilities. Nonetheless, our observation that about twice as much dietary TF-cholesterol can be localized to early endosomes (rab5c) at our early feeding time point (3 h) compared with rab7 and rab11a is consistent with the early endosomal compartment's receiving newly internalized materials first.

The observation of TF-cholesterol in recycling endosomes suggests that a subset of TF-cholesterol is targeted for exocytosis, either from the apical membrane into the intestinal lumen or from the basolateral membrane into the circulation. Cholesterol and plant sterols are secreted into the lumen by ABCG5/G8 to prevent cholesterol rising to toxic levels or the buildup of nonmetabolizable plant sterols; the majority of ABCG5/G8 localizes to the apical brush border of enterocytes, but some is found in unidentified intracellular punctae, which could plausibly be recycling endosomes (16). It is therefore possible that ABCG5/G8

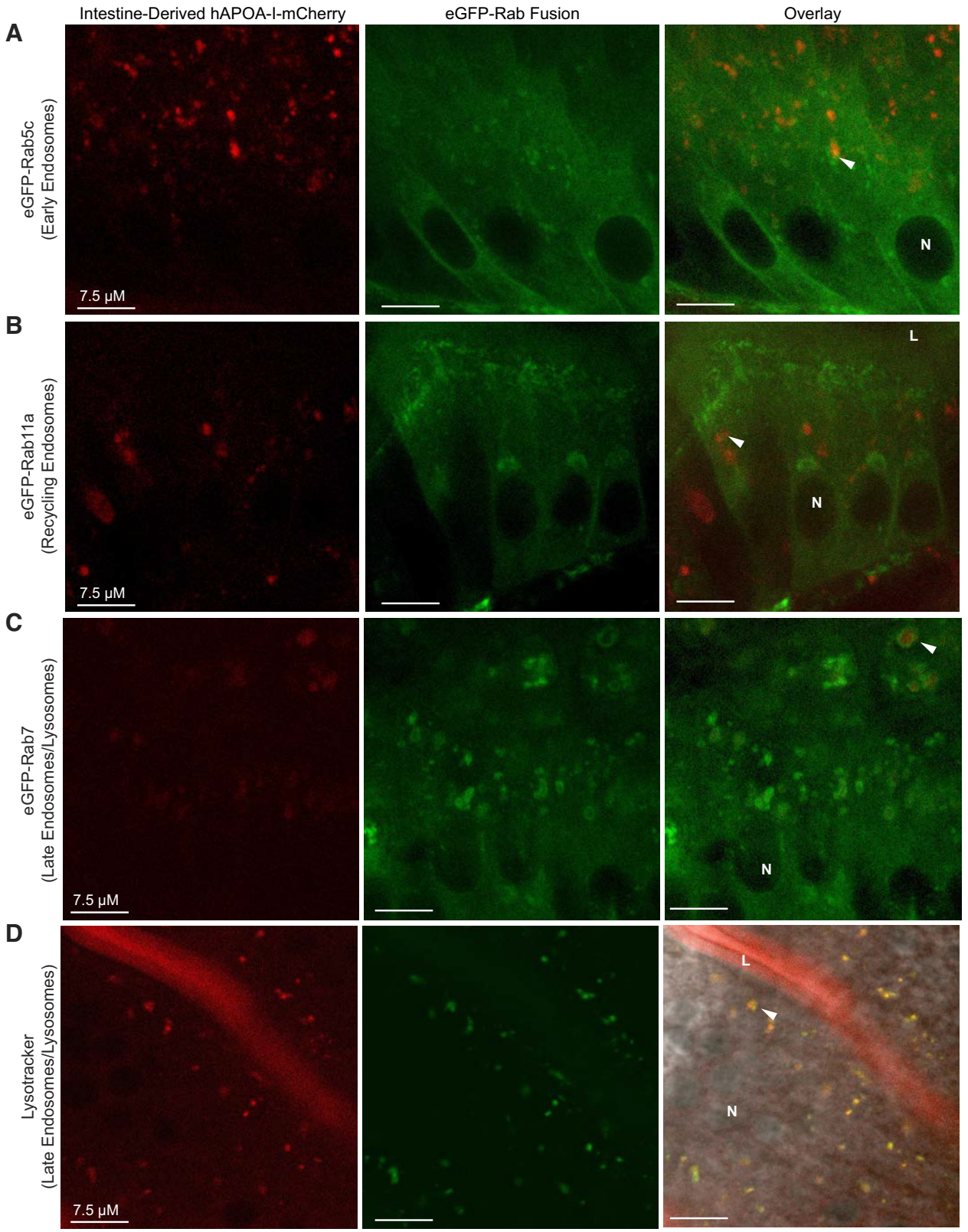

Fig. 6. hAPOA-I-mCherry localizes to the endosomal-lysosomal trafficking system in enterocytes of *tg(ifabp:hAPOA-I-mCherry)* larvae. Representative images demonstrate that hAPOA-I-mCherry colocalizes to early endosomes (*A*), recycling endosomes (*B*), and late endosomes/lysosomes, as marked by eGFP-Rab7 (*C*) and Lysotracker (*D*), in enterocytes. Arrowheads: colocalization; n = 3–4, with 3–12 fish per n, all fish 6-dpf. APOA-I, apolipoprotein A-I; dpf, days postfertilization; hAPOA-I, human APOA-I; L, intestinal lumen; N, nucleus.

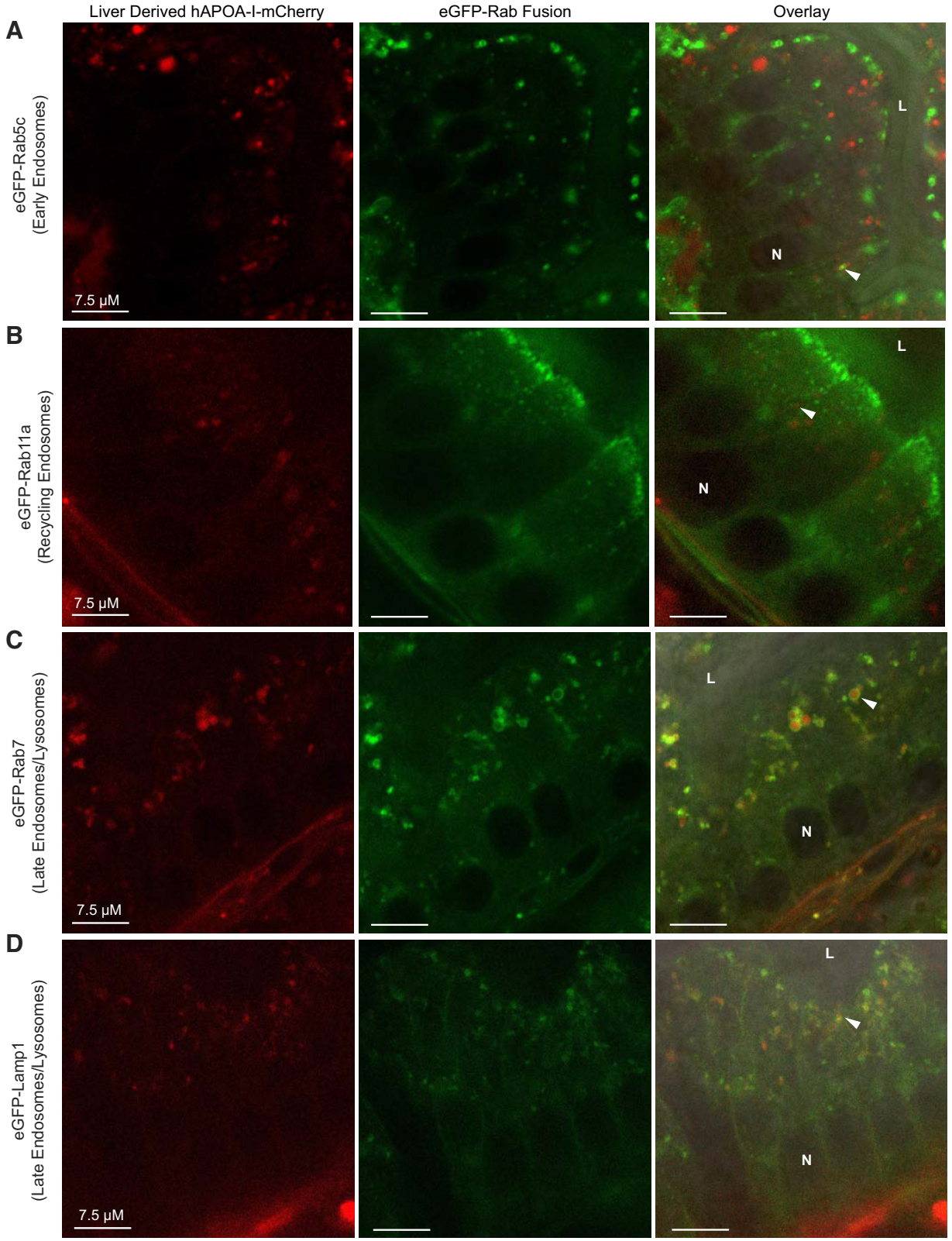

Fig. 7. hAPOA-I-mCherry localizes to the endosomal-lysosomal trafficking system in enterocytes of *tg(lfabp10:hAPOA-I-mCherry)* larvae. Representative images showing hAPOA-I-mCherry colocalized to early endosomes (eGFP-Rab5c) (*A*), recycling endosomes (eGFP-Rab11a) (*B*), late endosomes/lysosomes (eGFP-Rab7) (*C*), and lysosomes (eGFP-Lamp1) (*D*) in enterocytes. Arrowheads: colocalization; $n = 3–4$, with 3–12 fish per *n*. APOA-I, apolipoprotein A-I; hAPOA-I, human APOA-I; L, intestinal lumen; N, nucleus.

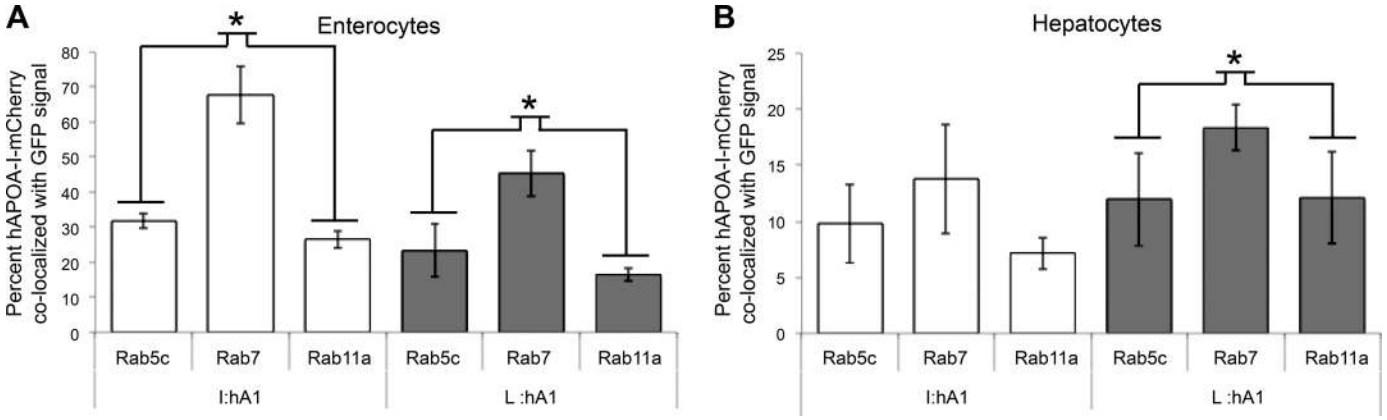

Fig. 8. Quantification of hAPOA-I-mCherry colocalization to endosomes and lysosomes in enterocytes (*A*) and hepatocytes (*B*). Quantitative assessment shows that hAPOA-I-mCherry colocalizes with markers of early, recycling, and late endosomes and lysosomes. Means ± SE, 1-way ANOVAs of *tg(ifabp:hAPOA-I-mCherry)* and *tg(lfabp10:hAPOA-I-mCherry)* groups, $*P < 0.05$, $n = 3–4$, with 3–12 fish per *n*. APOA-I, apolipoprotein A-I; GFP, green fluorescent protein; hAPOA-I, human APOA-I; I, hA1: *tg(ifabp:hAPOA-I-mCherry)*; L, hA1: *tg(lfabp10:hAPOA-I-mCherry)*.

localizes to recycling endosomes with dietary cholesterol, and part of the secretion process occurs at this location. An important consideration is that TF-cholesterol is not native cholesterol and may not fully replicate all aspects of cholesterol trafficking. Moreover, it remains unclear the degree to which ABCG5/G8 can interact with TF-cholesterol. These types of considerations must temper all studies using fluorescent lipid analogs.

In nonintestinal tissues, it has long been appreciated that exogenous cholesterol esters obtained from LDL uptake are trafficked through late endosomes to lysosomes for hydrolysis, before traveling to other cellular locations (9). This lysosomal processing constitutes an essential step in cholesterol metabolism in both normal and diseased states (7). Because our work shows dietary cholesterol trafficked through intestinal late endosomes and lysosomes, it is not surprising the Niemann-Pick type C disease is also associated with gastrointestinal symptoms and inflammation (12, 43). Moreover, cholesterol has been shown to play an important role in lysosomal nutrient sensing and autophagy (6, 28, 46).

Following the hydrolysis of LDL-derived cholesterol in the lysosome, free cholesterol is then rapidly exported from the lysosome to the ER for reesterification or to the Golgi for transport to the plasma membrane (9). Although our experimental method cannot distinguish the diffuse fluorescent signal of TF-cholesterol localized to the ER from background noise, we were able to detect TF-cholesterol in the Golgi by colocalization to BODIPY TR ceramides, suggesting dietary cholesterol may undergo similar vesicular trafficking in the intestine. The abundance of TF-cholesterol observed in the lateral and basolateral plasma membrane following feeding is consistent with a substantial fraction of this Golgi TF-cholesterol being targeted to the plasma membrane, where the majority of cellular free cholesterol resides (30).

NH_2-terminal fluorescent fusions of Rab proteins have been used previously to study endosomal function in both *Drosophila* (58) and zebrafish (10). In this study we used these previously reported fusion protein constructs except we used promoters with strong expression in 6-dpf zebrafish. We crossed these lines to each other and saw no colocalization of any of the Rab fusions (data not shown). However, because Rab proteins are important regulators of endosomal functions and facilitate communication between endosomes it is possible that their overexpression had unintended effects on endosomal/lysosomal function or morphology. It is for this reason that quantitative data we present might be influenced by the expansion of a specific Rab compartment as a result of overexpression, which could produce a subsequent increase in TF-cholesterol colocalization. Clarification of this issue will await the generation of zebrafish Rab-specific antibodies and the creation of fluorescent Rab transgenics with the fluorophore sequence inserted into the endogenous genomic locus.

The Rab fluorescent fusion proteins used in the study demonstrate the power of fluorescent fusions to study cell biology, yet very few studies have employed fluorescently tagged apolipoproteins. To our knowledge, only Yin et al. (56) expressed hAPOA-I-GFP in mice and observed its secretion from the liver into the circulation, similar to wild-type hAPOA-I overexpression (29). In our zebrafish model, hAPOA-I-mCherry and zApoA-Ia-mCherry (data not shown) exhibited similar distribution patterns to endogenous zApoA-Ia/b upon their secretion from the liver or intestine, highlighting their suitability for the study of APOA-I biology. It is not that surprising that in the organs that were producing the ApoA-I -mCherry, we did not observe diffuse ER/Golgi fluorescence, as might be expected for a secreted protein. We suspect this is because the protein is rapidly trafficked and not enough fluorescent molecules accumulate to be detected by conventional confocal microscopy. An additional open question is whether the hAPOA-I-mCherry and zApoA-Ia-mCherry fusions can generate nascent HDL particles or are preferentially incorporated into extant particles, something that further studies could address.

Both the intestine and liver synthesize HDL by ABCA1-mediated cellular cholesterol efflux to APOA-I, and ~30% of HDL in the circulation is of intestinal origin (3). The functions of HDL derived from the intestine versus the liver remain largely unstudied. Here, we created a system that allows for the identification of APOA-I from specific tissues by expressing hAPOA-I-mCherry and/or zApoA-Ia-mCherry on tissue-specific promoters. Although internalized APOA-I has been observed in the liver and intestine before, our model allowed us to make the astonishing finding that APOA-I-mCherry derived

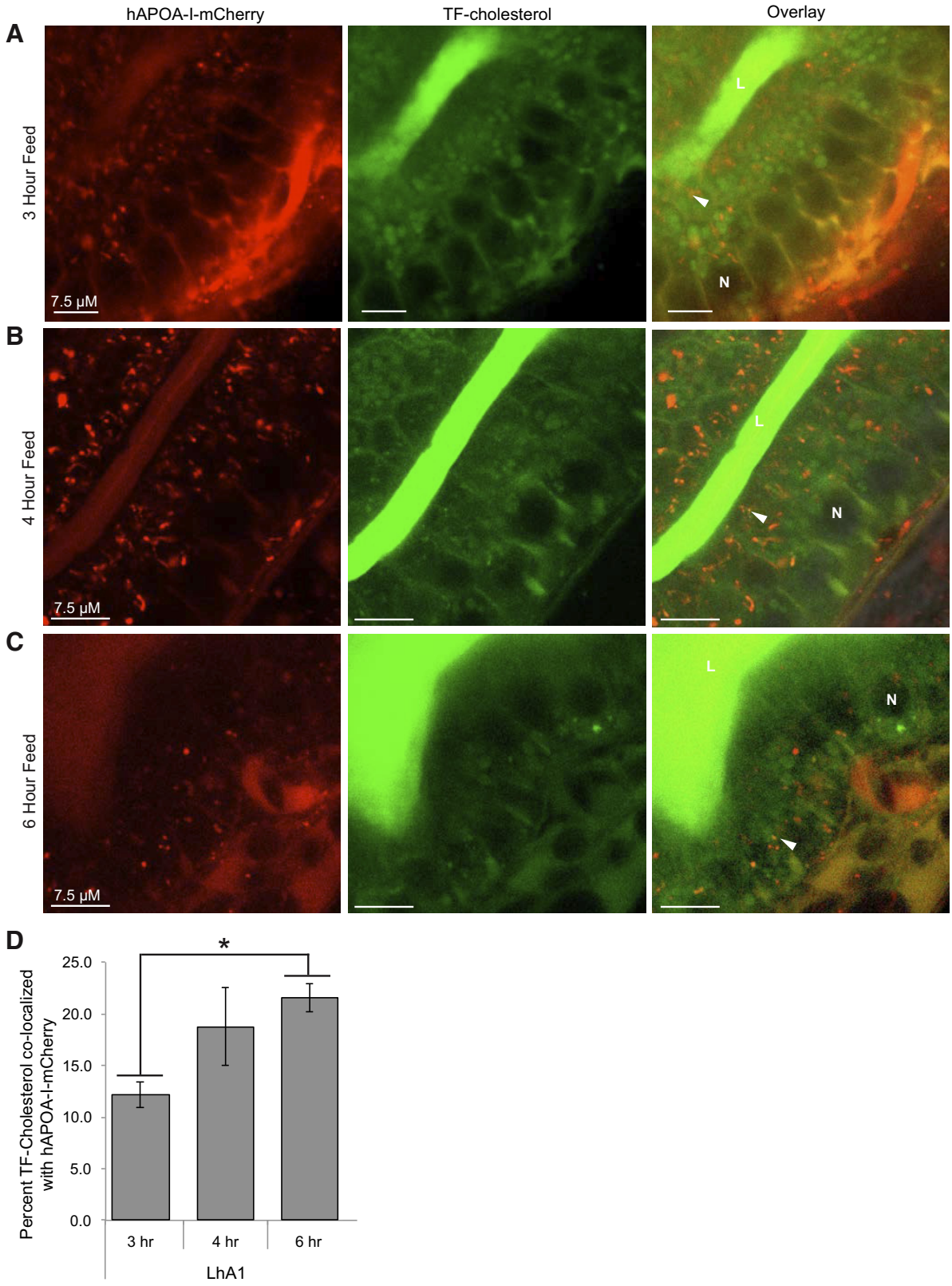

Fig. 9. hAPOA-I-mCherry colocalizes with dietary TF-cholesterol in enterocytes of *tg(lfabp10:hAPOA-I-mCherry)* larvae. Representative images showing hAPOA-I-mCherry and TF-cholesterol colocalization in enterocytes after 3 h (*A*), 4 h (*B*), and 6 h (*C*) of 5% egg yolk feed. Arrowheads: colocalization; n = 3–4, with 3–9 fish per n. A greater percent of TF-cholesterol colocalizes with hAPOA-I-mCherry at 6 h into feeding than at 3 h (means ± SE, 1-way ANOVA of *tg(lfabp10:hAPOA-I-mCherry)* groups, $^*P < 0.05$) (*D*). APOA-I, apolipoprotein A-I; hAPOA-I, human APOA-I; L, intestinal lumen; N, nucleus; TF-cholesterol, TopFluor-cholesterol.

from the intestine is internalized by hepatocytes and that APOA-I-mCherry of hepatic origin is taken up by enterocytes.

To interpret our data, it was essential to estimate the degree to which the observed fluorescence patterns result from the intact fusion proteins versus potential degradation products. To address this question, we first carried out Western blotting techniques using five commercially available mCherry antibodies; however, the antibodies did not recognize the intact APOA-I-mCherry fusion when the protein extract was denatured using standard immunoblot protocols. Indeed, many proteins that interact with lipids have previously been shown to require specialized immunoblotting techniques for detection. For example, Sabeva et al. (40) performed SDS-PAGE and immunoblot analysis of ABCA1 (an ApoA-I and lipid-binding protein) using a loading buffer containing 3% SDS. This approach, modified with 37°C heating of the protein extract, enabled us to observe the APOA-I-mCherry fusion product using the mCherry antibody. In contrast, the ApoA-I antibody reveals only the intact fusion protein of the expected size in larval extracts using standard denaturing conditions. Our native gel methods of assaying fluorescence avoid these problems and results reveal that 60–100% of the fluorescence is derived from the full-length fusion protein and the degree of degradation depends on the specific transgenic line. Not surprisingly, the more strongly overexpressing line has greater evidence of degradation. In sum, the observation that fluorescence is observed in lysosomal compartments is consistent with degradation occurring after cellular uptake.

The finding that hAPOA-I-mCherry accumulates in endosomes and lysosomes in the live intestine and liver validates previous observations of these localizations in cultured cells and fixed tissues. However, because most APOA-I lipidation and cholesterol efflux to HDL is thought to occur at the plasma membrane, it was less expected to see hAPOA-I-mCherry and TF-cholesterol colocalization in endosomes. This observation supports the theory that APOA-I/HDL may be modified by ABCA1 and/or scavenger receptor BI intracellularly. Further studies are needed to understand the physiological role of this intracellular ApoA-I.

In conclusion, we leveraged the power of the larval zebrafish to provide evidence consistent with cholesterol being transported through the endosomal/lysosomal system in the intestine. Moreover, analysis of the localization of the APOA-I-mCherry fluorescent fusion protein suggests that APOA-I from the intestine is taken up in the liver and vice versa. Within these tissues, APOA-I was shown to be trafficked in endosomes and localize to lysosomes. Finally, our cholesterol feeding assay allowed for the visualization of APOA-I colocalization with dietary cholesterol in the intestine.

ACKNOWLEDGMENTS

We are grateful to Brian Link and Michel Bagnat for providing plasmids; Mahmud Siddiqi for assistance with image analysis and comments on the manscript; Jennifer Anderson for advice on the statistical analysis; Meredith Wilson for helpful discussion; and Kasia Hussey, Maggie Shen, and Monica Hensley for technical assistance. Thanks to James Walters and Juliana Carten who performed pilot experiments relevant to the larval zebrafish fluorescent cholesterol feeding protocol.

GRANTS

This work was supported by National Institutes of Health (NIH) Grant F32-DK-096786 (to J. P. Otis), RO1-DK-093399 and R01-DK-116079 (to S. A. Farber), and RO1-GM-63904 (The Zebrafish Functional Genomics Consortium: Principal Investigator Stephen Ekker and Coprincipal Investigator S. A. Farber). Additional support for this work was provided by the Carnegie Institution for Science Endowment and the G. Harold and Leila Y. Mathers Charitable Foundation.

DISCLAIMERS

This content is solely the responsibility of the authors and does not necessarily represent the official views of NIH.

DISCLOSURES

No conflicts of interest, financial or otherwise, are declared by the authors.

AUTHOR CONTRIBUTIONS

J.P.O. and S.A.F. conceived and designed research; J.P.O., M.-C.S., B.A.C., O.E.R.G., and S.A.F. performed experiments; J.P.O., M.-C.S., B.A.C., O.E.R.G., and S.A.F. analyzed data; J.P.O., M.-C.S., B.A.C., O.E.R.G., and S.A.F. interpreted results of experiments; J.P.O., M.-C.S., B.A.C., and S.A.F. prepared figures; J.P.O. and S.A.F. drafted manuscript; J.P.O., B.A.C., O.E.R.G., and S.A.F. edited and revised manuscript; J.P.O., M.-C.S., B.A.C., O.E.R.G., and S.A.F. approved final version of manuscript.

REFERENCES

1. **Ahras M, Naing T, McPherson R.** Scavenger receptor class B type I localizes to a late endosomal compartment. *J Lipid Res* 49: 1569–1576, 2008. doi:10.1194/jlr.M800055-JLR200.
2. **Altmann SW, Davis HR JR, Zhu LJ, Yao X, Hoos LM, Tetzloff G, Iyer SP, Maguire M, Golovko A, Zeng M, Wang L, Murgolo N, Graziano MP.** Niemann-Pick C1 Like 1 protein is critical for intestinal cholesterol absorption. *Science* 303: 1201–1204, 2004. doi:10.1126/science.1093131.
3. **Brunham LR, Kruit JK, Iqbal J, Fievet C, Timmins JM, Pape TD, Coburn BA, Bissada N, Staels B, Groen AK, Hussain MM, Parks JS, Kuipers F, Hayden MR.** Intestinal ABCA1 directly contributes to HDL biogenesis in vivo. *J Clin Invest* 116: 1052–1062, 2006. doi:10.1172/JCI27352.
4. **Carten JD, Bradford MK, Farber SA.** Visualizing digestive organ morphology and function using differential fatty acid metabolism in live zebrafish. *Dev Biol* 360: 276–285, 2011. doi:10.1016/j.ydbio.2011.09.010.
5. **Carten JD, Farber SA.** A new model system swims into focus: using the zebrafish to visualize intestinal metabolism in vivo. *Clin Lipidol* 4: 501–515, 2009. doi:10.2217/clp.09.40.
6. **Castellano BM, Thelen AM, Moldavski O, Feltes M, van der Welle RE, Mydock-McGrane L, Jiang X, van Eijkeren RJ, Davis OB, Louie SM, Perera RM, Covey DF, Nomura DK, Ory DS, Zoncu R.** Lysosomal cholesterol activates mTORC1 via an SLC38A9-Niemann-Pick C1 signaling complex. *Science* 355: 1306–1311, 2017. doi:10.1126/science.aag1417.
7. **Chang TY, Reid PC, Sugii S, Ohgami N, Cruz JC, Chang CC.** Niemann-Pick type C disease and intracellular cholesterol trafficking. *J Biol Chem* 280: 20917–20920, 2005. doi:10.1074/jbc.R400040200.
8. **Chen W, Sun Y, Welch C, Gorelik A, Leventhal AR, Tabas I, Tall AR.** Preferential ATP-binding cassette transporter A1-mediated cholesterol efflux from late endosomes/lysosomes. *J Biol Chem* 276: 43564–43569, 2001. doi:10.1074/jbc.M107938200.
9. **Storch J, Cheruku SR.** Cholesterol transport in lysosomes. In: *Lysosomes. Medical Intelligence Unit*. Boston: Springer, 2005.
10. **Clark BS, Winter M, Cohen AR, Link BA.** Generation of Rab-based transgenic lines for in vivo studies of endosome biology in zebrafish. *Dev Dyn* 240: 2452–2465, 2011. doi:10.1002/dvdy.22758.
11. **Dietschy JM, Gamel WG.** Cholesterol synthesis in the intestine of man: regional differences and control mechanisms. *J Clin Invest* 50: 872–880, 1971. doi:10.1172/JCI106559.
12. **Dinari G, Rosenbach Y, Grunebaum M, Zahavi I, Alpert G, Nitzan M.** Gastrointestinal manifestations of Niemann-Pick disease. *Enzyme* 25: 407–412, 1980. doi:10.1159/000459289.
13. **Eckhardt ER, Cai L, Sun B, Webb NR, van der Westhuyzen DR.** High density lipoprotein uptake by scavenger receptor SR-BII. *J Biol Chem* 279: 14372–14381, 2004. doi:10.1074/jbc.M313793200.
14. **Fu J, Bonder MJ, Cenit MC, Tigchelaar EF, Maatman A, Dekens JA, Brandsma E, Marczynska J, Imhann F, Weersma RK, Franke L, Poon TW, Xavier RJ, Gevers D, Hofker MH, Wijmenga C, Zhernakova A.** The gut microbiome contributes to a substantial proportion of the

variation in blood lipids. *Circ Res* 117: 817–824, 2015. doi:10.1161/CIRCRESAHA.115.306807.
15. **Galvez T, Gilleron J, Zerial M, O'Sullivan GA.** SnapShot: mammalian Rab proteins in endocytic trafficking. *Cell* 151: 234–234, 2012.
16. **Graf GA, Yu L, Li WP, Gerard R, Tuma PL, Cohen JC, Hobbs HH.** ABCG5 and ABCG8 are obligate heterodimers for protein trafficking and biliary cholesterol excretion. *J Biol Chem* 278: 48275–48282, 2003. doi:10.1074/jbc.M310223200.
17. **Grant BD, Donaldson JG.** Pathways and mechanisms of endocytic recycling. *Nat Rev Mol Cell Biol* 10: 597–608, 2009. doi:10.1038/nrm2755.
18. **He C, Klionsky DJ.** Analyzing autophagy in zebrafish. *Autophagy* 6: 642–644, 2010. doi:10.4161/auto.6.5.12092.
19. **Hölttä-Vuori M, Uronen RL, Repakova J, Salonen E, Vattulainen I, Panula P, Li Z, Bittman R, Ikonen E.** BODIPY-cholesterol: a new tool to visualize sterol trafficking in living cells and organisms. *Traffic* 9: 1839–1849, 2008. doi:10.1111/j.1600-0854.2008.00801.x.
20. **Hui DY, Howles PN.** Molecular mechanisms of cholesterol absorption and transport in the intestine. *Semin Cell Dev Biol* 16: 183–192, 2005. doi:10.1016/j.semcdb.2005.01.003.
21. **Ikonen E.** Cellular cholesterol trafficking and compartmentalization. *Nat Rev Mol Cell Biol* 9: 125–138, 2008. doi:10.1038/nrm2336.
22. **Jäckle S, Rinninger F, Lorenzen T, Greten H, Windler E.** Dissection of compartments in rat hepatocytes involved in the intracellular trafficking of high-density lipoprotein particles or their selectively internalized cholesteryl esters. *Hepatology* 17: 455–465, 1993.
23. **Jones B, Jones EL, Bonney SA, Patel HN, Mensenkamp AR, Eichenbaum-Voline S, Rudling M, Myrdal U, Annesi G, Naik S, Meadows N, Quattrone A, Islam SA, Naoumova RP, Angelin B, Infante R, Levy E, Roy CC, Freemont PS, Scott J, Shoulders CC.** Mutations in a Sar1 GTPase of COPII vesicles are associated with lipid absorption disorders. *Nat Genet* 34: 29–31, 2003. doi:10.1038/ng1145.
24. **Kambouris AM, Roach PD, Calvert GD, Nestel PJ.** Retroendocytosis of high density lipoproteins by the human hepatoma cell line, HepG2. *Arteriosclerosis* 10: 582–590, 1990. doi:10.1161/01.ATV.10.4.582.
25. **Kang MH, Singaraja R, Hayden MR.** Adenosine-triphosphate-binding cassette transporter-1 trafficking and function. *Trends Cardiovasc Med* 20: 41–49, 2010. doi:10.1016/j.tcm.2010.03.006.
26. **Kimmel CB, Ballard WW, Kimmel SR, Ullmann B, Schilling TF.** Stages of embryonic development of the zebrafish. *Dev Dyn* 203: 253–310, 1995. doi:10.1002/aja.1002030302.
27. **Kwan KM, Fujimoto E, Grabher C, Mangum BD, Hardy ME, Campbell DS, Parant JM, Yost HJ, Kanki JP, Chien CB.** The Tol2kit: a multisite gateway-based construction kit for Tol2 transposon transgenesis constructs. *Dev Dyn* 236: 3088–3099, 2007. doi:10.1002/dvdy.21343.
28. **Laplante M, Sabatini DM.** mTOR signaling at a glance. *J Cell Sci* 122: 3589–3594, 2009. doi:10.1242/jcs.051011.
29. **Li Y, Dong JB, Wu MP.** Human ApoA-I overexpression diminishes LPS-induced systemic inflammation and multiple organ damage in mice. *Eur J Pharmacol* 590: 417–422, 2008. doi:10.1016/j.ejphar.2008.06.047.
30. **Liscum L, Faust JR.** Compartmentation of cholesterol within the cell. *Curr Opin Lipidol* 5: 221–226, 1994. doi:10.1097/00041433-199405030-00010.
31. **Luo J, Jiang L, Yang H, Song BL.** Routes and mechanisms of post-endosomal cholesterol trafficking: A story that never ends. *Traffic* 18: 209–217, 2017. doi:10.1111/tra.12471.
32. **Luzio JP, Hackmann Y, Dieckmann NM, Griffiths GM.** The biogenesis of lysosomes and lysosome-related organelles. *Cold Spring Harb Perspect Biol* 6: a016840, 2014. doi:10.1101/cshperspect.a016840.
33. **Mansbach CM II, Abumrad NA.** *Enterocyte fatty acid handling proteins and chylomicron formation*. In: *Physiology of the Gastrointestinal Tract*. 2 vols. Elsevier, 2012, p. 1625–1641. doi:10.1016/B978-0-12-382026-6.00060-9.
34. **Maxfield FR, McGraw TE.** Endocytic recycling. *Nat Rev Mol Cell Biol* 5: 121–132, 2004. doi:10.1038/nrm1315.
35. **Neufeld EB, Remaley AT, Demosky SJ, Stonik JA, Cooney AM, Comly M, Dwyer NK, Zhang M, Blanchette-Mackie J, Santamarina-Fojo S, Brewer HB JR.** Cellular localization and trafficking of the human ABCA1 transporter. *J Biol Chem* 276: 27584–27590, 2001. doi:10.1074/jbc.M103264200.
36. **Otis JP, Farber SA.** High-fat feeding paradigm for larval zebrafish: feeding, live imaging, and quantification of food intake. *J Vis Exp* (116): 2016. doi:10.3791/54735.
37. **Otis JP, Zeituni EM, Thierer JH, Anderson JL, Brown AC, Boehm ED, Cerchione DM, Ceasrine AM, Avraham-Davidi I, Tempelhof H, Yaniv K, Farber SA.** Zebrafish as a model for apolipoprotein biology: comprehensive expression analysis and a role for ApoA-IV in regulating food intake. *Dis Model Mech* 8: 295–309, 2015. doi:10.1242/dmm.018754.
38. **Rogler G, Herold G, Stange EF.** HDL3-retroendocytosis in cultured small intestinal crypt cells: a novel mechanism of cholesterol efflux. *Biochim Biophys Acta* 1095: 30–38, 1991. doi:10.1016/0167-4889(91)90041-U.
39. **Röhrl C, Pagler TA, Strobl W, Ellinger A, Neumüller J, Pavelka M, Stangl H, Meisslitzer-Ruppitsch C.** Characterization of endocytic compartments after holo-high density lipoprotein particle uptake in HepG2 cells. *Histochem Cell Biol* 133: 261–272, 2010. doi:10.1007/s00418-009-0672-3.
40. **Sabeva NS, Rouse EJ, Graf GA.** Defects in the leptin axis reduce abundance of the ABCG5-ABCG8 sterol transporter in liver. *J Biol Chem* 282: 22397–22405, 2007. doi:10.1074/jbc.M702236200.
41. **Sasahara T, Kobori S, Kasho M, Sato Y, Nishikawa T, Yano T, Takeda H, Shichiri M.** The metabolic fate of apolipoprotein A-I-containing lipoproteins internalized into HepG2 cells: resecreted lipoproteins as a potent inducer for cholesterol efflux. *Atherosclerosis* 106: 179–190, 1994. doi:10.1016/0021-9150(94)90123-6.
42. **Schwend T, Loucks EJ, Ahlgren SC.** Visualization of Gli activity in craniofacial tissues of hedgehog-pathway reporter transgenic zebrafish. *PLoS One* 5: e14396, 2010. doi:10.1371/journal.pone.0014396.
43. **Schwerd T, Pandey S, Yang HT, Bagola K, Jameson E, Jung J, Lachmann RH, Shah N, Patel SY, Booth C, Runz H, Düker G, Bettels R, Rohrbach M, Kugathasan S, Chapel H, Keshav S, Elkadri A, Platt N, Muise AM, Koletzko S, Xavier RJ, Marquardt T, Powrie F, Wraith JE, Gyrd-Hansen M, Platt FM, Uhlig HH.** Impaired antibacterial autophagy links granulomatous intestinal inflammation in Niemann-Pick disease type C1 and XIAP deficiency with NOD2 variants in Crohn's disease. *Gut* 66: 1060–1073, 2017. doi:10.1136/gutjnl-2015-310382.
44. **Semova I, Carten JD, Stombaugh J, Mackey LC, Knight R, Farber SA, Rawls JF.** Microbiota regulate intestinal absorption and metabolism of fatty acids in the zebrafish. *Cell Host Microbe* 12: 277–288, 2012. doi:10.1016/j.chom.2012.08.003.
45. **Settembre C, Ballabio A.** Lysosome: regulator of lipid degradation pathways. *Trends Cell Biol* 24: 743–750, 2014. doi:10.1016/j.tcb.2014.06.006.
46. **Settembre C, Zoncu R, Medina DL, Vetrini F, Erdin S, Erdin S, Huynh T, Ferron M, Karsenty G, Vellard MC, Facchinetti V, Sabatini DM, Ballabio A.** A lysosome-to-nucleus signalling mechanism senses and regulates the lysosome via mTOR and TFEB. *EMBO J* 31: 1095–1108, 2012. doi:10.1038/emboj.2012.32.
47. **Silbernagel G, Chapman MJ, Genser B, Kleber ME, Fauler G, Scharnagl H, Grammer TB, Boehm BO, Mäkelä KM, Kähönen M, Carmena R, Rietzschel ER, Bruckert E, Deanfield JE, Miettinen TA, Raitakari OT, Lehtimäki T, März W.** High intestinal cholesterol absorption is associated with cardiovascular disease and risk alleles in ABCG8 and ABO: evidence from the LURIC and YFS cohorts and from a meta-analysis. *J Am Coll Cardiol* 62: 291–299, 2013. doi:10.1016/j.jacc.2013.01.100.
48. **Silver DL, Wang N, Tall AR.** Defective HDL particle uptake in ob/ob hepatocytes causes decreased recycling, degradation, and selective lipid uptake. *J Clin Invest* 105: 151–159, 2000. doi:10.1172/JCI8087.
49. **Soccio RE, Breslow JL.** Intracellular cholesterol transport. *Arterioscler Thromb Vasc Biol* 24: 1150–1160, 2004. doi:10.1161/01.ATV.0000131264.66417.d5.
50. **Swerdlow PS, Finley D, Varshavsky A.** Enhancement of immunoblot sensitivity by heating of hydrated filters. *Anal Biochem* 156: 147–153, 1986. doi:10.1016/0003-2697(86)90166-1.
51. **Sylvén C, Borgström B.** Intestinal absorption and lymphatic transport of cholesterol in the rat: influence of the fatty acid chain length of the carrier triglyceride. *J Lipid Res* 10: 351–355, 1969.
52. **Thisse C, Thisse B.** High-resolution in situ hybridization to whole-mount zebrafish embryos. *Nat Protoc* 3: 59–69, 2008. doi:10.1038/nprot.2007.514.
53. **Tóth IE, Szabó D, Bácsy E, Szalay KS, Hesz A, Szollár LG.** Morphological evidence of lysosomal uptake of high-density lipoproteins by rat adrenocortical cells in vitro. *Mol Cell Endocrinol* 44: 185–194, 1986. doi:10.1016/0303-7207(86)90062-6.
54. **Wang DQ.** Regulation of intestinal cholesterol absorption. *Annu Rev Physiol* 69: 221–248, 2007. doi:10.1146/annurev.physiol.69.031905.160725.
55. **Wüstner D, Mondal M, Huang A, Maxfield FR.** Different transport routes for high density lipoprotein and its associated free sterol in polar-

ized hepatic cells. *J Lipid Res* 45: 427–437, 2004. doi:10.1194/jlr.M300440-JLR200.

56. **Yin K, Tang SL, Yu XH, Tu GH, He RF, Li JF, Xie D, Gui QJ, Fu YC, Jiang ZS, Tu J, Tang CK.** Apolipoprotein A-I inhibits LPS-induced atherosclerosis in ApoE(-/-) mice possibly via activated STAT3-mediated upregulation of tristetraprolin. *Acta Pharmacol Sin* 34: 837–846, 2013. doi:10.1038/aps.2013.10.

57. **Young SC, Hui DY.** Pancreatic lipase/colipase-mediated triacylglycerol hydrolysis is required for cholesterol transport from lipid emulsions to intestinal cells. *Biochem J* 339: 615–620, 1999. doi:10.1042/bj3390615.

58. **Zhang J, Schulze KL, Hiesinger PR, Suyama K, Wang S, Fish M, Acar M, Hoskins RA, Bellen HJ, Scott MP.** Thirty-one flavors of Drosophila rab proteins. *Genetics* 176: 1307–1322, 2007. doi:10.1534/genetics.106.066761.